CrossMark

A detector setup for the measurement of angular distribution of heavy-ion elastic scattering with low energy on RIBLL

Gao-Long Zhang[1] · Yong-Jin Yao[1] · Guang-Xin Zhang[1] · Zhen-Wei Jiao[1] ·
Cheng-Jian Lin[2] · Ya-Zhou Niu[1] · Wei-Wei Qu[3] · Lei Yang[2] · Nan-Rou Ma[2] ·
Lei Zheng[1] · Hui-Ming Jia[2] · Li-Jie Sun[2] · Xing-Xing Liu[1] · Xiao-Tong Chu[1] ·
Jie-Cheng Yang[1] · Jian-Song Wang[4] · Shi-Wei Xu[4] · Peng Ma[4] · Jun-Bing Ma[4] ·
Shi-Lun Jin[4] · Zhen Bai[4] · Mei-Rong Huang[4] · Hong-Liang Zang[5] ·
Biao Yang[5] · Yang Liu[5]

Abstract A detector setup for the measurement of angular distribution of heavy-ion elastic scattering at energies around Coulomb barrier on the radioactive ion beam line in Lanzhou at the heavy-ion research facility in Lanzhou is designed. The beam profile and the scattering angles on the target are deduced by two parallel plate avalanche counters, and four sets of detector telescopes (including double-sided silicon strip detectors) are placed systematically with the beam line, incorporating with Monte Carlo simulations. The data of ^{16}O on ^{89}Y target were analyzed to compare with the simulation results. It is found that the simulated distribution is agreeable with the experimental data. By assuming the pure Rutherford scattering at small scattering angles, the angular distribution of elastic scattering of ^{16}O + ^{89}Y at low energies can be reasonably obtained. It indicates that this set of detector setup can be used for the measurement of angular distributions of heavy-ion elastic scattering at energies around Coulomb barrier.

Keywords Angular distribution · Low-energy heavy ion · Monte Carlo · RIBLL

✉ Gao-Long Zhang
zgl@buaa.edu.cn

✉ Cheng-Jian Lin
cjlin@ciae.ac.cn

1 School of Physics and Nuclear Energy Engineering, Beihang University, Beijing 100191, China

2 China Institute of Atomic Energy, Beijing 102413, China

3 School of Radiation Medicine and Protection, Medical College of Soochow University, Soochow 215123, China

4 Institute of Modern Physics, Chinese Academy of Sciences, Lanzhou 730000, China

5 School of Physics and State Key Laboratory of Nuclear Physics and Technology, Peking University, Beijing 100871, China

1 Introduction

Elastic scattering is an important tool to explore the inner structure of nuclei and reaction mechanisms. Based on the analysis of the elastic scattering angular distributions, the optical potentials and the reaction mechanisms can be studied. In particular, recently the availability of radioactive ion beam (RIB) facilities in a few laboratories [1–6] makes it possible for scientists to learn more about the nuclear structure and different reaction phenomena from elastic scattering.

The precise measurement of elastic scattering angular distribution is a crucial task. A series of collimators is required to collimate the beam spot along with the beam line, and several sets of large area detectors are employed to measure the beam trajectory before the secondary target since the beam spot of RIB is much larger than that of stable beam. Because of its high energy and spatial resolution, double-sided silicon strip detector (DSSD) is often used for the measurement of the scattered particles. Some of silicon strip detectors, such as EXPADES detector array [7] and compact disk (CD) double-sided silicon strip detector array [8], are used for elastic scattering experiments. These detectors can measure the angular distributions of heavy-ion elastic scatterings at energies around the Coulomb barrier well. If the beam spot size and emittance on the target are small enough, the scattering angle of each

particle can be directly obtained from the geometry relationship between the fired silicon strip and the beam spot. However, if the beam spot size and emittance on the target are not negligible compared with the distance between the target and the detectors, the angles of particles need to be tracked event by event and cannot be directly obtained by silicon strips only.

This experiment was performed on the radioactive ion beam line in Lanzhou (RIBLL) which was designed as a double-achromatic anti-symmetry separator. RIBLL was constructed at the heavy-ion research facility of Lanzhou (HIRFL) [9, 10] and has been in operation since 1998. It is a kind of projectile fragmentation (PF)-type RIB separator with a large momentum acceptance and solid angle. The value of the beam emittance, which is designed to be 50 mm mrad in both X and Y directions, is actually 30 and 40 mm mrad in X and Y directions, respectively, for the secondary beam on the secondary target position [11]. There are three focal points (T0, T1 and T2) under achromatic mode and two focal planes (C1, C2) where the horizontal momentum dispersion ($\Delta x/\Delta p/p$) is about 20 mm%. Detailed information about it can be learned from Refs. [12, 13]. Recently a new low-energy radioactive beam line for nuclear astrophysics studies on the basis of RIBLL was developed [14]. In order to perform the heavy-ion nuclear reaction at low energy on this beam line and study the mechanisms of nuclear reactions at energies around Coulomb barrier, a primary beam ^{17}O was employed to produce the secondary beam containing ^{16}O. However, since PF-type separator has a broad distribution in coordinate space, it is difficult to obtain the accurate cross sections of elastic scattering by a high statistics measurement when small collimator is used to produce the well-defined beam. In this paper, the scattered events of ^{16}O + ^{89}Y are selected to check whether this detector setup can measure the angular distributions of elastic scattering at energies around Coulomb barrier.

2 Experimental setup

The primary beam ^{17}O with a beam intensity of 1 μA was accelerated up to 7.6 MeV/u and passed through a 21 μm aluminum foil, and then bombarded a H_2 gas target which was installed at T0 of RIBLL. The gas was confined into a cylindrical cell with $\phi 30$ windows and a length of 80 mm. The forward and backward windows were covered by Havar foils with a thickness of 2.5 μm. The gas cell was cooled around $5°$ by water-cooling system, and the gas pressure was kept around 600 Torr. The generated secondary beam was separated, purified and transported by RIBLL to secondary target chamber at T2. At T1 and T2

two plastic scintillators (C_9H_{10}) with the thickness of 10 μm were installed in the beam line to give the time of flight (TOF) information. More detailed information about low-energy RIBs is given in Ref. [14]. Two parallel plate avalanche counters (PPACs) were installed at the location of 1666 and 1285 mm in front of the secondary target ^{89}Y. Therefore, the beam position on the secondary target can be determined by analyzing the two-dimensional hit positions measured by two PPACs. The two collimators with $\phi 30$ were installed behind the two PPACs and in front of the secondary target to limit the beam spot. The secondary target ^{89}Y with a thickness of 0.981 mg/cm^2 was tilted at $65°$ with respect to the beam line. Around the ^{89}Y target four sets of $\Delta E-E$ detector telescopes were symmetrically mounted along the beam direction and covered the angular range of $15°-115°$ (Fig. 1). The square silicon detectors (SSD) with 300 μm in thickness and 50 mm × 50 mm in area are mounted behind DSSDs with 65 μm in thickness and 50 mm × 50 mm in area as well as 3 mm strip width and 0.1 mm the strip span.

3 Measurements

3.1 Particle identification

Two processes were performed in the experiment. Firstly, a silicon detector with a thickness of 300 μm was inserted into the beam line between PPAC2 and the plastic scintillation detector at T2 as an E detector to stop the beam. The plot of E-TOF for beam particle identification is shown in Fig. 2. Since the flight distance is fixed, with the calibration values of TOF and the total kinetic energy E, each beam component can be distinguished (marked in Fig. 2). Depending on the magnetic rigidity $B\rho$ set for the last dipole magnet D4, the energy of each component can be estimated. Then the calibrated energies are compared to the estimated ones in order to check their validity. In this way, it is found that the present calibrated components correspond to the experimental data. So we can tell the identification of beam particles is reliable.
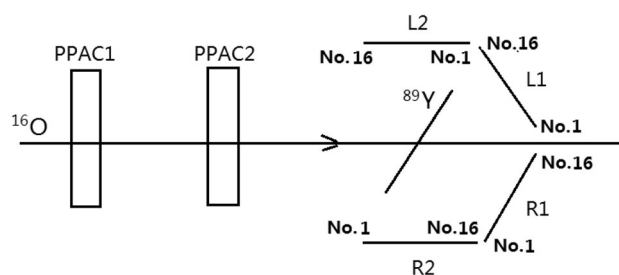

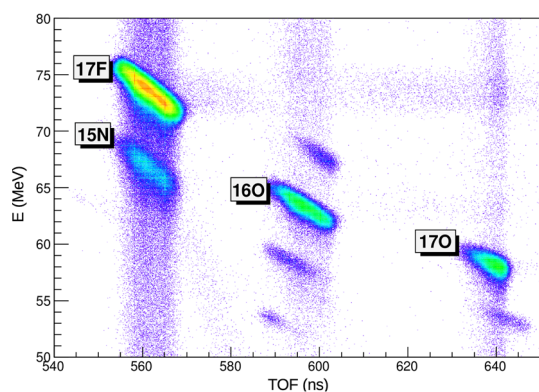Fig. 1 Schematic view of detector setup of this experiment

Fig. 2 (Color online) Plot of E-TOF for beam particle identification

Secondly, the silicon detector was removed from the beam line. Therefore, TOF signal is essential for particle identification. Figure 2 shows that there are large differences of TOF among ^{16}O, ^{17}F and ^{17}O, so that the events of incident ^{17}F and ^{17}O can be excluded by selecting a correct TOF window. Meanwhile, ^{16}O and the other components have a similar TOF value as shown in Fig. 2. However, due to the significant energy differences, none of the other scattered components can be mixed into the scattered ^{16}O events on the energy spectrum of scattering particles. Since ^{16}O has a large energy difference in comparison with ^{17}F and ^{17}O, it is still possible for ^{16}O to be distinguished from the energy spectrum of DSSDs without TOF windows. In practice, the secondary beam includes a lot of unexpected components in RIB experiments. For our case, in cooperation with TOF signals, the precision of our experimental results can be improved.

3.2 The distributions of particles on PPAC and DSSD

In the experiment, due to the large beam spot of secondary beam on the target, the trajectories of particles have to be tracked one by one. In order to achieve this goal, two PPACs are mounted at the secondary target ^{89}Y.

PPAC is often used in the nuclear reaction experiments because of its many advantages such as good position resolution, large sensitive area and easy to fabricate. It is composed of two anode planes and one cathode plane. All electrode planes are put in parallel to assure the uniformity of electric field. The cathode plane which is made of Mylar foil coated with a thin gold layer on both sides lies in the middle of PPAC. The two anode planes which are made of gold-plated tungsten wires are symmetrically positioned on both sides of the cathode plane. Both the entrance and exit windows are covered by Mylar foils with about 12 μm in thickness and the grids made of fishing line support the Mylar foils to resist high gas pressure. The wires on both

two anode planes with a sensitive area of 80 mm × 80 mm are perpendicular to each other to give the X and Y direction positions. There are 80 wires on X and Y directions, respectively. The span between each two wires is 1 mm for each direction. The signals of wire electrodes are connected to each other by delay cables. The time difference between two readout signals of the anode planes gives the position information of beam particles.

Figure 3a, b presents the distributions of incident ^{16}O on PPAC1 and PPAC2. The spot on PPAC2 is smaller than that on PPAC1, which corresponds to the fact that T2 is a focal point. This demonstrates that this set of PPACs can reflect the beam trajectory and precisely give the position coordinates of each particle on PPAC1 and PPAC2. Then the incident points on ^{89}Y target can be determined. It is important to determine the scattering angle of each particle.

The distributions of scattered ^{16}O on two DSSDs (L1 and R1 placed symmetrically with the beam line) are shown in Fig. 4. According to the sequences of silicon strips which are shown in Fig. 1, for L1, the silicon strips from No. 1 to No. 16 correspond to angles from forward to backward. For R1, the silicon strips from No. 1 to No. 16 correspond to angles from backward to forward. On the basis of kinematic principle, the energies of scattered particles at forward angles are larger than those at backward angles as shown in Fig. 4a, b. This means that the present DSSDs can give the kinematic trends of scattered particles. The scattering angle of each particle can be obtained event by event.

Figure 5 indicates the experimental angular distribution of scattered ^{16}O on ^{89}Y target (solid line). It is shown that in the ranges of 20°–60° and over 80°, with the increase in scattering angles, the number of events decreases. However, around 65° a sudden decrease occurs due to the influence of target and the connection position of the detectors which is described in Fig. 1 and Section II. The experimental results correspond to the geometry of detector
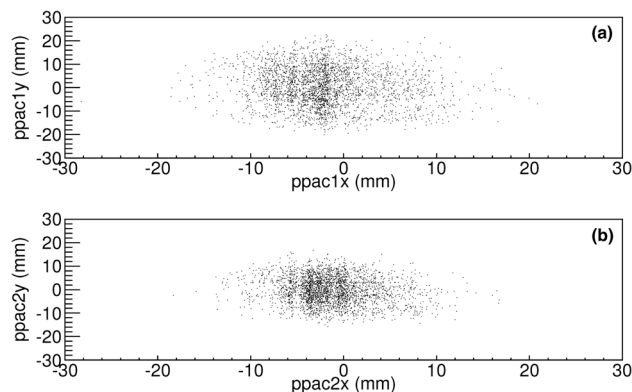

Fig. 3 (Color online) Distributions of incident ^{16}O on PPACs. **a** on PPAC1; **b** on PPAC2

Fig. 4 (Color online) Distributions of scattered ^{16}O on DSSD. The *horizontal axis* denotes the channels of X-strips of DSSD. **a** L1; **b** R1
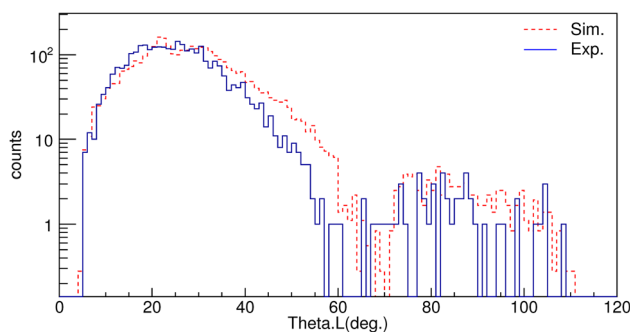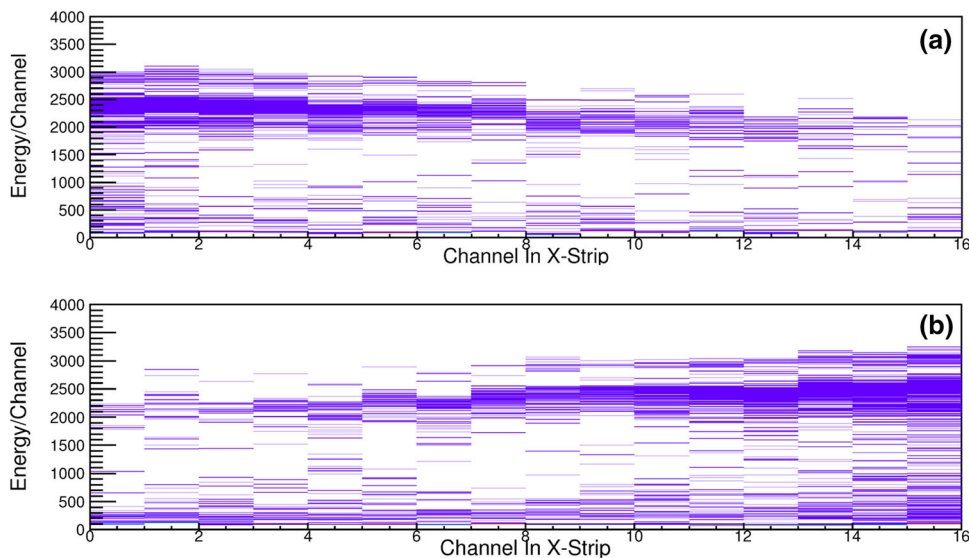
Fig. 5 (Color online) Angular distributions of ^{16}O on ^{89}Y target as a function of scattering angles. The *solid and dashed lines* represent the experimental data and the simulation results, respectively

setup. Therefore, the determination of scattering angles is acceptable. The present DSSDs can not only give the reasonable kinematic trends of scattered particles, but also provide the precise angular information of scattered particles.

3.3 Simulation

In the angular distribution of elastic scattering, the differential cross sections of this reaction are normalized to the differential cross sections of Rutherford scattering. The ratios are plotted as a function of scattering angles. Since the beam spots of RIBs on the target cannot be viewed as a point with respect to the distance between the target and the detector, the Monte Carlo method is applied to simulate the Rutherford scattering. In the simulation program, we took into account (1) the kinematics of elastic scattering process; (2) the energy spread of the secondary beam; (3) the Gaussian distributed beam spot with $\sigma = 6.5$ mm on the target; (4) the real geometry design of detector system; (5)

the energy loss in the target evaluated by TRIM code [15]. In addition, the reaction position along the beam direction inside the target is random. The simulation results are shown in Fig. 5 (dashed line). It is observed that the inflection position is almost identical. Therefore, the simulation method and results are reasonable.

3.4 Results and discussions

The ratios of reaction differential cross sections to the differential cross sections of Rutherford scattering are obtained by

$$\frac{\mathrm{d}\sigma(\theta)}{\mathrm{d}\sigma_{Ru}(\theta)} = C\frac{N(\theta)}{N_{Ru}(\theta)}, \tag{1}$$

where the parameter C is a normalization constant which is determined by supposing that the elastic scattering is a pure Rutherford scattering in a region of small scattering angles (much smaller than the grazing angle). $N(\theta)$ and $N_{Ru}(\theta)$ are the elastic scattering events and Rutherford scattering events with the same solid angle at any scattering angle θ in the frame of laboratory system, respectively. In this experiment, at an laboratory angle θ, $N(\theta)$ is the experimental counts of ^{16}O scattering on ^{89}Y target and $N_{Ru}(\theta)$ is obtained from the Monte Carlo simulation.

For ^{16}O at 50 MeV, the experimental scattering events are normalized to the simulation events at the angle of 22° where the elastic scattering is expected to be a pure Rutherford scattering. The results are shown in Fig. 6 as a function of scattered angles in the laboratory frame. Here only statistic error is considered. It presents that in the ranges of 10°–35° and 75°–110° the ratios almost keep the unity. Because at this energy, the scattering of ^{16}O on ^{89}Y target is pure Rutherford scattering. It demonstrates that the
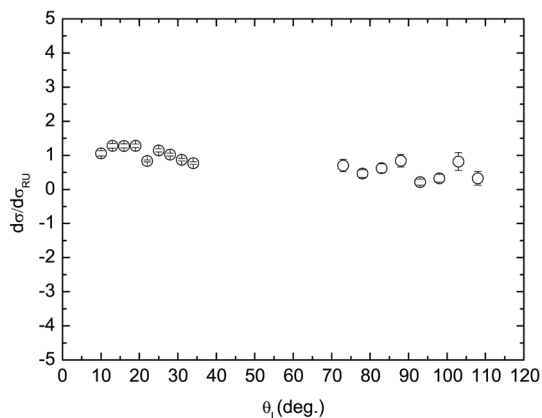
Fig. 6 Angular distribution of elastic scattering of $^{16}O + ^{89}Y$ at 50 MeV

normalized method is reasonable. This detection system can effectively determine the elastic scattering angular distributions and give the precise angular calibration.

In summary, for this detector setup, PPACs can precisely determine the beam trajectories before the target and DSSDs can correctly determine the positions of scattered particles. The deduced scattering angles are reasonable. The simulation about Rutherford scattering is correct. The normalization results of elastic scattering angular distributions can prove that the angular calibration is precise. As a result, this detector setup can be used for the study of heavy-ion elastic scattering at energies around Coulomb barrier on HIRFL-RIBLL.

References

1. Y. Yanagisawa, S. Kubono, T. Teranishi et al., Low-energy radioisotope beam separator CRIB. Nucl. Instrum. Methods Phys. Res. Sect. A **539**, 74–83 (2005). doi:10.1016/j.nima.2004.09.041
2. F. Farinon, T. Glodariu, M. Mazzocco et al., Commissioning of the EXOTIC beam line. Nucl. Instrum. Methods Phys. Res. Sect. B **26**, 4097–4102 (2008). doi:10.1016/j.nimb.2008.05.128
3. M.Y. Lee, F.D. Becchetti, T.W. O'Donnell et al., Study of nuclear reactions with intense, high-purity, low energy radioactive ion beams using a versatile multi-configuration dual superconducting-solenoid system. Nucl. Instrum. Methods Phys. Res. Sect. A **422**, 536–540 (1999). doi:10.1016/S0168-9002(98)01081-X
4. B. Harss et al., in Proceedings of the XVIII International Linear Accelerator Conference, Geneva, Switzerland, CERN 96-072, 496 (1996)
5. K.A. Li, Y.L. Ye, Recent development in experimental RIB physics. Nucl. Tech. **37**(10), 100501 (2014). doi:10.11889/j.0253-3219.2014.hjs.37.100501. (in Chinese)
6. S. Wang, Electron scattering facility for short-lived nuclei at RIKEN. Nucl. Tech. **37**(10), 100523 (2014). doi:10.11889/j.0253-3219.2014.hjs.37.100523
7. E. Strano, A. Anastasio, M. Bettini et al., The high granularity and large solid angle detection array EXPADES. Nucl. Instrum. Methods Phys. Res. Sect. B **317**, 657–660 (2013). doi:10.1016/j.nimb.2013.06.035
8. A.N. Ostrowski, S. Cherubini, T. Davinson et al., CD: a double sided silicon strip detector for radioactive nuclear beam experiments. Nucl. Instrum. Methods Phys. Res. Sect. A **480**, 448–455 (2002). doi:10.1016/S0168-9002(01)00954-8
9. J.W. Xia, W.L. Zhan, B.W. Wei et al., The heavy ion cooler-storage-ring project (HIRFL-CSR) at Lanzhou. Nucl. Instrum. Methods Phys. Res. Sect. A **488**, 11–25 (2002). doi:10.1016/S0168-9002(02)00475-8
10. W.L. Zhan, H.S. Xu, G.Q. Xiao et al., Progress in HIRFL-CSR. Nucl. Phys. A **834**, 694c–700c (2010). doi:10.1016/j.nuclphysa.2010.01.126
11. Y.Y. Yang, J.S. Wang, Q. Wang et al., A method for the measurement of elastic scattering angular distribution at HIRFL-RIBLL. Nucl. Instrum. Methods Phys. Res. Sect. A **701**, 1–6 (2013). doi:10.1016/j.nima.2012.10.088
12. Z.Y. Sun, W.L. Zhang, Z.Y. Guo et al., Separation and identification of isotopes produced from $^{20}Ne + Be$ reaction by radioactive ion beam line in Lanzhou. Chin. Phys. Lett. **15**(11), 790 (1998). doi:10.1088/0256-307X/15/11/004
13. Z.Y. Sun, W.L. Zhan, Z.Y. Guo et al., RIBLL, the radioactive ion beam line in Lanzhou. Nucl. Instrum. Methods Phys. Res. Sect. A **503**, 496 (2003). doi:10.1016/S0168-9002(03)01005-2
14. J.J. He, S.W. Xu, P. Ma et al., A new low-energy radioactive beam line for nuclear astrophysics studies in China. Nucl. Instrum. Methods Phys. Res. Sect. A **680**, 43–47 (2012). doi:10.1016/j.nima.2012.03.040
15. J.F. Ziegler et al., *The Stopping and Range of Ions in Solids* (Pergamon Press, Oxford, 1985)